JOURNAL OF GEOPHYSICAL RESEARCH, VOL. 114, F02011, doi:10.1029/2008JF001082, 2009

Mass balance of the Prince of Wales Icefield, Ellesmere Island, Nunavut, Canada

Douglas Mair,[1] David Burgess,[2] Martin Sharp,[3] Julian A. Dowdeswell,[4] Toby Benham,[4] Shawn Marshall,[5] and Fiona Cawkwell[6]

Received 28 May 2008; revised 3 February 2009; accepted 23 February 2009; published 29 April 2009.

[1] This paper estimates the mass balance of the Prince of Wales Icefield, Ellesmere Island, Canada, averaged over four decades, from measurements of surface mass balance (SMB) and iceberg calving. Shallow ice core net accumulation measurements and annual mass balance stake measurements are used in conjunction with a digital elevation model and knowledge of the location of the dominant moisture source for precipitation over the ice cap to interpolate and extrapolate spatial patterns of SMB across the Prince of Wales Icefield. The contribution of iceberg calving to the mass balance is calculated from estimates of (1) the annual volume of ice discharged at the major tidewater glacier termini and (2) the annual volume loss or gain due to terminus fluctuations. Two different approaches to determining the SMB conclude that the SMB of the ice field is approximately in balance (average equals -0.1 ± 0.4 km^3 w.e. a^{-1}, where w.e. means water equivalent) largely because of its proximity to the main year-round moisture source that is the Smith Sound portion of the North Open Water polynya. Iceberg calving is a highly significant component of mass loss (-1.9 ± 0.2 km^3 w.e. a^{-1}) and is sufficient to make the overall mass balance of the ice field averaged over the period 1963–2003 clearly negative (-2 ± 0.45 km^3 w.e. a^{-1}, equivalent to a mean-specific mass balance across the ice field of -0.1 m w.e. a^{-1}). The Prince of Wales Icefield contributes $\sim$0.005 mm a^{-1} to global eustatic sea level rise.

Citation: Mair, D., D. Burgess, M. Sharp, J. A. Dowdeswell, T. Benham, S. Marshall, and F. Cawkwell (2009), Mass balance of the Prince of Wales Icefield, Ellesmere Island, Nunavut, Canada, *J. Geophys. Res.*, *114*, F02011, doi:10.1029/2008JF001082.

1. Introduction

[2] With $\sim$110,000 km^2 glacier ice, [*Dowdeswell et al.*, 1997] the Canadian High Arctic contains the greatest area of land ice outside the Greenland and Antarctic Ice Sheets. Global climate models consistently predict that anthropogenic climate warming will be strongest at high northern latitudes [*Intergovernmental Panel on Climate Change*, 2007], and there is evidence that resultant cryospheric changes may be under way [e.g., *Dowdeswell et al.*, 1997; *Paterson and Reeh*, 2001; *Burgess and Sharp*, 2004]. From 1961 to 2003 the ice caps and ice fields of the Canadian Arctic contributed 8% of the total global sea level rise that could be attributed to the melting of ice caps and glaciers [*Dyurgerov and Meier*, 2005]. Current estimates are, however, based on the results of mass balance monitoring of a relatively small number of generally small ice masses, and there is only limited information about the extent and causes of ice cap area and volume change in the region [*Burgess and Sharp*, 2004, 2008; *Burgess et al.*, 2005; *Mair et al.*, 2005; *Abdalati et al.*, 2004; *Williamson et al.*, 2008]. It is important to obtain as comprehensive a picture as possible of the recent and current mass balance status of these large ice caps, and those in other parts of the Arctic [*Dowdeswell et al.*, 2002, 2008], in order to assess their contribution to recent global sea level rise and predict the contribution that may be expected over the coming decades and centuries.

[3] In this paper, we aim to estimate the overall mass balance of the Prince of Wales Icefield (POW), central Ellesmere Island, Canada (Figure 1), averaged over four decades, from the sum of surface mass balance (SMB) and iceberg calving. Shallow ice core measurements of long-term net SMB from the accumulation area are combined with annual mass balance stake measurements that span the entire elevation range of the ice field to determine the potential spatial pattern of SMB. The contribution of iceberg calving to the overall mass balance is calculated from estimates of (1) the ice flux discharged at the major tidewater glacier termini and (2) the volume loss or gain due to observed changes in the positions of glacier termini.

[1]Department of Geography and Environment, School of Geosciences, University of Aberdeen, Aberdeen, UK.
[2]Canada Centre for Remote Sensing, Natural Resources Canada, Ottawa, Ontario, Canada.
[3]Department of Earth and Atmospheric Sciences, University of Alberta, Edmonton, Alberta, Canada.
[4]Scott Polar Research Institute, University of Cambridge, Cambridge, UK.
[5]Department of Geography, University of Calgary, Calgary, Alberta, Canada.
[6]Department of Geography, University College Cork, Cork, UK.

0148-0227/09/2008JF001082$09.00

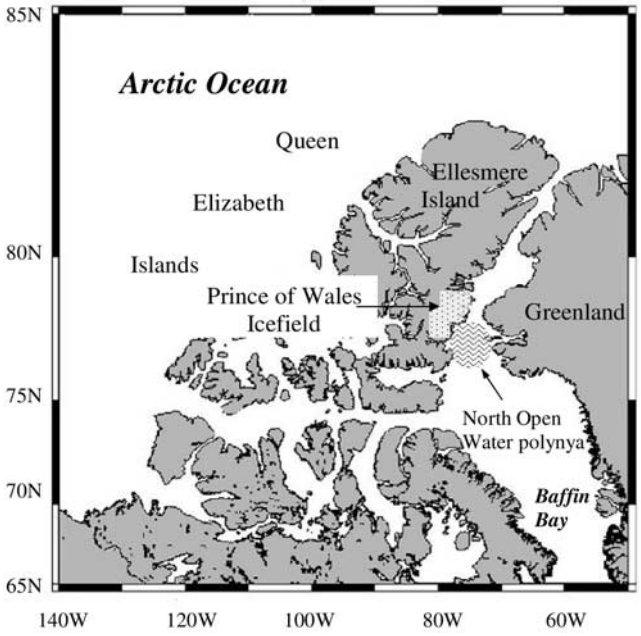

Figure 1. Location of the Prince of Wales Icefield on Ellesmere Island, Nunavut, Canada. Also shown is the Smith Sound portion of the North Open Water (NOW) polynya.

[4] An immediate challenge in our attempts to determine the average mass balance of a large ice cap comes from the variety of time scales that available observations and measurements cover. Although we hereafter refer to the period 1963–2003 as the long-term period over which we estimate mass balance, it should be stated from the outset that none of our individual measurements cover this specific time period but rather, they encompass or overlap with varying fractions of this period. Herein, we aim to determine realistic error bars for the mass balance estimate that reflect both field measurement and sampling errors and uncertainties in extrapolating and interpolating information over variable temporal and spatial scales. This research is part of an integrated study of the area/volume change and dynamics of the Canadian Arctic ice caps [*Burgess and Sharp*, 2004, 2008; *Dowdeswell et al.*, 2004; *Mair et al.*, 2005; *Burgess et al.*, 2005; *Colgan et al.*, 2008; *Williamson et al.*, 2008].

2. Field Site

[5] The Prince of Wales Icefield (POW), Ellesmere Island, Nunavut, Canada (Figures 1 and 2) is a High Arctic ice field with an area of 19,325 km^2. In several locations, nunataks and snow covered mountains protrude to elevations of over 2000 m above sea level (asl) above a broad, gently sloping central plateau ranging in altitude from ca. 1350 to 1730 m asl. The ice field descends to sea level on the east coast of Ellesmere Island, but terminates on land on the western margin, at altitudes from 400 to 600 m asl. This asymmetry results from a strong east-west gradient in snow accumulation over the ice field that is caused by southeasterly storm tracks from Baffin Bay sweeping across the North Open Water (NOW) Polynya [*Koerner*, 1977, 1979]. The Smith Sound portion of the NOW is centered to the southeast of POW, providing a major source of moisture for the ice field. Most of the NOW polynya is kept open by the latent heat mechanism which involves the mechanical removal of ice by currents and winds south of an ice bridge that forms across northern Smith Sound in winter, preventing ice from the Arctic from entering the polynya [*Mundy and Barber*, 2001]. *Steffen* [1985] provided evidence that the Smith Sound portion of the NOW polynya may be kept open by coastal upwelling of warm, deep Baffin Bay water of Atlantic origin.

[6] Although POW is the second largest ice mass in the Canadian High Arctic, few glaciological measurements have been carried out on the ice field [*Koerner*, 1977, 1979], and POW is not included in the mass balance monitoring program conducted by the Geological Survey of Canada [*Koerner*, 2005]. Thus, this paper presents the first mass balance measurements from POW in over 25 years.

3. Field Measurements and Data Sources

[7] Detailed descriptions of the measurements and errors associated with each mass balance component follow below, but Table 1 summarizes the time periods covered by measurements of the terms that appear in the overall mass balance estimate. Unavoidable assumptions and uncertainties about the representativeness of our measurements for the period 1963–2003 are inherent in the necessity to combine separate mass balance components measured over different time periods. When measuring surface mass balance, for example, long-term average accumulation can be closely constrained by stratigraphic measurements on shallow ice cores made at any point in time. However, ablation measurements relate specifically to the time period over which stakes have been emplaced and subsequently revisited and measured. Hence annual ablation stake measurements may be less representative of the long-term ablation pattern than are ice core measurements of the accumulation pattern. Estimating the long-term average mass loss through iceberg calving is subject to similar problems. Calving margins can fluctuate by hundred of meters seasonally [*Joughin et al.*, 2008] and annual calving can change significantly as the ice and bed geometry of the changing terminus region evolves [*O'Neel et al.*, 2005]. Thus an accurate long-term calving flux estimate must include long-term observations of ice marginal change. Ice flux to a glacier terminus can also vary over a range of timescales, and so a velocity value based on repeat satellite image analyses over just a few weeks or days combined with snapshots of ice thickness made at one or two moments in time may not be truly representative of ice dynamics averaged over several decades.

[8] Furthermore, our estimate of mass balance does not include any consideration of the effect of basal melt (or accretion) on the underside of floating tidewater termini. Basal melting has been shown to be a major source of mass loss from floating ice masses in Antarctica [*Rignot and Jacobs*, 2002] and Greenland [*Rignot and Steffen*, 2008]. Airborne ice thickness measurements (see below) suggest that grounding lines are currently located within a maximum of 3 km from tidewater termini, so POW does not

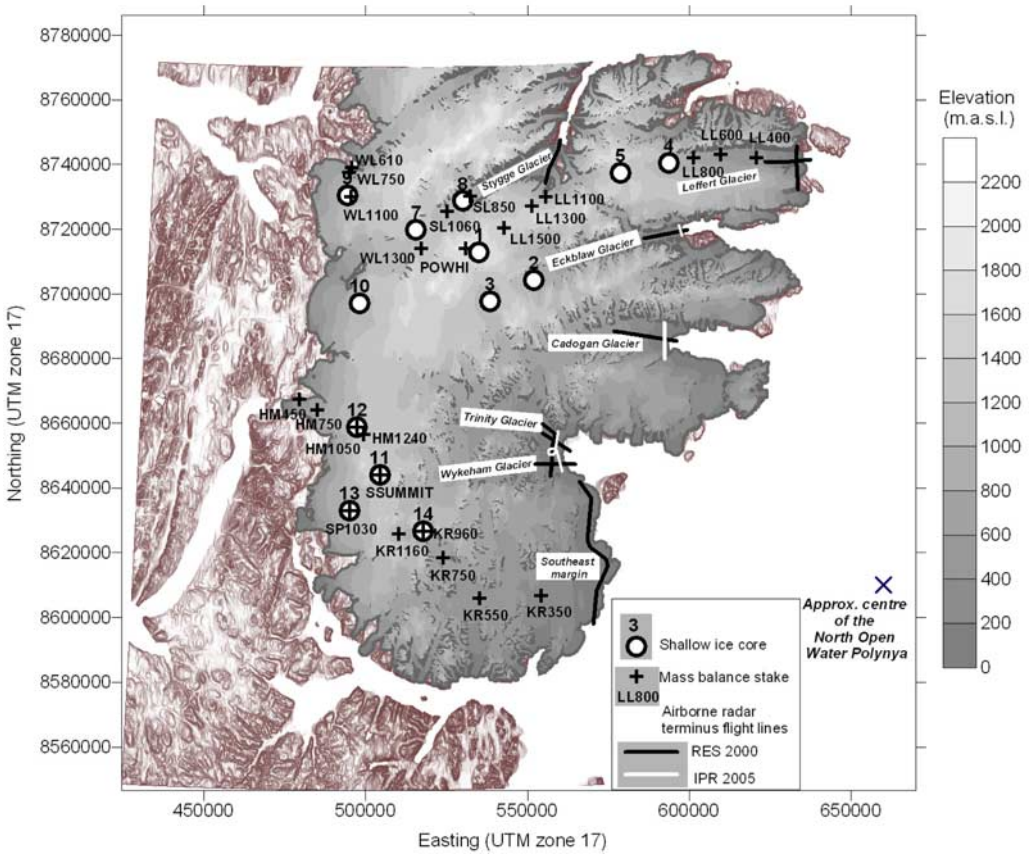

Figure 2. DEM and location of field measurements of the Prince of Wales Icefield. The CDED data set used did not include data north of 79°N. Less than 3% of the total surface area of the ice field is missing from the SMB interpolations. The missing portion ranges in elevation from over 1500 m to sea level. Note that exclusion of this area, which encompasses accumulation and ablation areas, from subsequent SMB interpolations will have a negligible impact on B_n values, and any minor effect will lie well within quantifiable error bounds.

have extensive floating tongues. There is also no evidence that warm ocean currents reach the coast of Ellesmere Island and the tidewater glaciers of POW. We assume that bottom melting is therefore not a major source of mass loss from POW.

3.1. Surface Mass Balance

3.1.1. Measurements of Net Accumulation From Shallow Ice Cores

[9] In April–May 2001 and 2002, 13 shallow cores were drilled across the accumulation areas of POW, at elevations ranging from 941 m to 1730 m above sea level (Figure 2). Coring sites were located on (1) the interior plateau (sites 1, 3 and 11); (2) three major outlet glaciers, the Leffert Glacier (sites 4 and 5), the Ekblaw Glacier (site 2) and the Stygge Glacier (sites 7 and 8); (3) catchments draining to the northwest margin (sites 9 and 10); (4) catchments draining to the southwest margin (sites 12 and 13); and (5) within the complex topography of the southeast catchments (site 14). The Kovacs Mark II ice corer used in this study produced cores with diameters of 9 cm and average lengths of ~40 cm. Snow and firn densities were determined immediately after

Table 1. Time Period Covered by Measurements of Terms Appearing in the Overall Long-Term Average Mass Balance Estimate, Notionally 1963–2003

Components of Overall Mass Balance	Measurement/Observation Time Period
Net accumulation	
Northern cores	1963–2000
Southern cores	1963–2001
Net surface ablation	May 2002 to May 2003
Ice flux at glacier termini	
Surface velocities	24 day averages from Nov–Dec 2000 (Cadogan Glacier), Feb–Mar 2003 (Ekblaw Glacier), and Feb–Mar 2004 (Trinity and Wykeham glaciers) [*Short and Gray*, 2005]
Ice thicknesses	10 April 2000 and 5 May 2005
Changes in ice marginal positions	July 1959/August 1960 to July 1999/August 2000

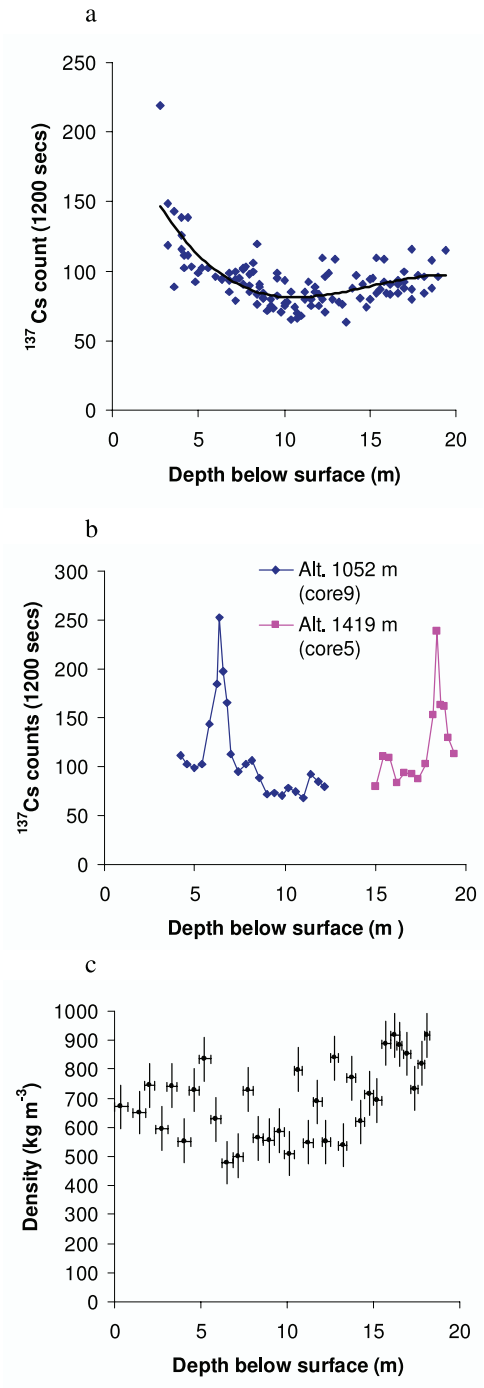

Figure 3. (a) Composite scatterplot of ^{137}Cs against depth of northern core sites excluding peaks at depth. Polynomial fit is used as a reference for calculating anomalous ^{137}Cs readings. (b) Here ^{137}Cs against depth for sites 5 and 9 showing clear bomb layer peak at depth. (c) Example of depth/density profile from core at site 7, 1234 m elevation. The estimated error in individual firn density measurements is ±75 kg m^{-3}.

retrieval of cores by measuring the diameter, length and weight of each core section.

[10] Using a down-borehole gamma spectrometer (NaI(TI) detector with photomultiplier tube and MicroMCB multichannel analyzer software), gamma activity profiles of boreholes produced by removal of each shallow core were measured using a method similar to that described by *Dunphy and Dibb* [1994] and identical to that described by *Mair et al.* [2005]. Gamma emission counts accumulated over 1200 s were made for the energy bands of a ^{109}Cd reference source, ^{137}Cs and two other spectral intervals. Counts were conducted at 40 cm intervals, working upward from the bottom of each borehole. Profiles for all spectral intervals except ^{109}Cd showed an exponential increase toward the surface (Figure 3a) that was likely due to cosmic ray-produced gamma rays [*Dunphy and Dibb*, 1994]. The count profiles for ^{137}Cs showed a secondary peak at depth (e.g., Figure 3b) that was associated with peak fallout from atmospheric testing of thermonuclear weapons in 1962–63. Profiling resolution was increased to 20-cm intervals around this peak to determine its location more accurately. Using the depths of the 1963 radioactive fallout layer and measurements of the densities of firn and snow above this layer (e.g., Figure 3c), the net mass balance averaged over the period 1963–2000/2001, $b_{n\ 63-00/01}$, was calculated for each core site. The estimated error of these measurements is discussed in the Results section below.

3.1.2. Stake Measurements

[11] From May 2002 to May 2003, measurements were made of changes in the depths of winter snow and previous summer firn or ice surfaces across a network of mass balance stakes deployed along two transects across the ice field (Figure 2). The northern transect ranges in elevation from 130 m to 2010 m above sea level and includes sites on the interior plateau, the Leffert and Stygge Glaciers, and catchments draining to the northwest margin. The southern transect ranges in elevation from 350 m to 1350 m above sea level. It extends from the southeastern margin to the southern summit and descends to 450 m above sea level in catchments draining to the western and southwestern margins. Measurements of snow surface (relative to the top of each stake, stk_d), snow pit depths (from snow surface to previous summer surface, sn_d), snow densities (ρ_{sn}), previous summer firn densities (in the accumulation area, ρ_{fn}), and an assumed glacier ice density of 900 kg m^{-3} (in the ablation area, ρ_i) were used to calculate net SMB for the year May 2002 to May 2003 ($b_{n\ 02-03}$), at 24 locations across the ice field, where

$$b_{n02-03} = \rho_{sn}(sn_{d1} - sn_{d0}) + \rho_{fn/i}[(stk_{d0} + sn_{d0}) - (stk_{d1} + sn_{d1})], \quad (1)$$

where subscripts, t = 0 and 1 refer to May 2002 and May 2003 respectively.

[12] These measurements take account of melting and refreezing that is likely to have occurred within the annual snowpack during summer 2002. We cannot, however, preclude the possibility that surface melt may have percolated below the annual layer in which case our estimate of b_n will be erroneously low. This source of error is more likely at lower elevations within the accumulation area. We estimate the error in these stake measurements to be 10–15%.

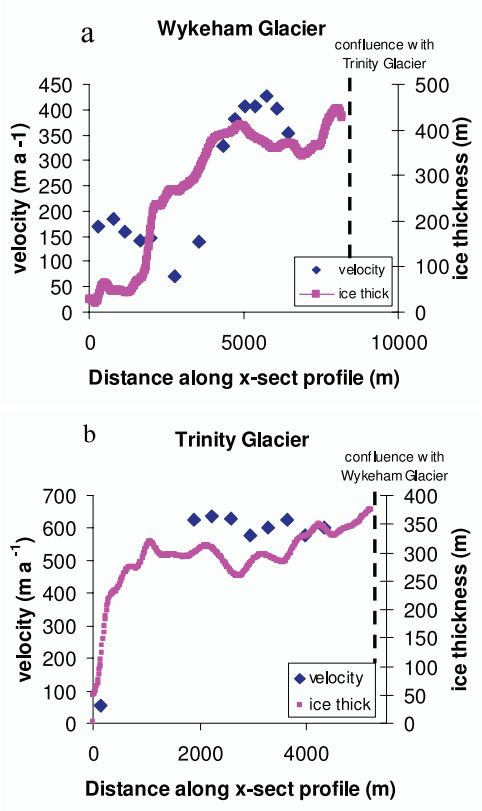

Figure 4. Ice thickness and surface velocity of (a) Wykeham Glacier and (b) Trinity Glacier.

3.2. Iceberg Calving Rates

[13] Following *Burgess et al.* [2005], the annual discharge of ice calved from tidewater glaciers was calculated as

$$Q_{Total} = Q_{flux} + Q_{v-loss}, \quad (2)$$

where Q_{flux} is the annual volume of ice discharged at tidewater termini and Q_{v-loss} is the volume loss due to observed changes in the terminus positions of tidewater outlet glaciers. To determine Q_{Total} we need to know the cross-sectional area, A_{x-sect}, and average cross-sectional velocity, $\bar{v}_{x-\mathrm{sect}}$, of the ice at the terminus of each outlet glacier and the history of terminus advance or retreat. Errors in Q_{Total} are a consequence of measurement errors in ice thickness and surface velocity and of limitations in the spatial and temporal sampling of ice thickness and surface velocity measurements. These are now discussed in relation to A_{x-sect}, $\bar{v}_{x-\mathrm{sect}}$ and Q_{v-loss}.

3.2.1. Cross-Sectional Area, A_{x-sect}: Measurement and Errors

[14] Airborne radio echo sounding (RES) measurements at 100 MHz were made along longitudinal flight lines following the centerline of the main east flowing tidewater glaciers in 2000. RES measurements were acquired at time intervals equating to ~7.5 m intervals along track. The estimated error in ice thickness is ±10 m. The acquisition and analyses of these measurements is identical to that described by *Dowdeswell et al.* [2004]. Ice thicknesses at the center point of transverse cross sections of calving tidewater glacier termini were determined from these measurements. In May 2005, similar measurements were made by the University of Kansas ice-penetrating radar (IPR) system mounted on a Twin Otter aircraft that flew transects across the termini of the three most dynamic east flowing tidewater glaciers, the Ekblaw, Cadogan and Trinity/Wykeham glaciers (Figure 2). Data points along these profiles were acquired at ~12 m intervals. *Short and Gray* [2005] calculated iceberg calving rates for some of the major tidewater terminating glaciers draining the eastern margin of POW, however their estimates were limited by a lack of cross-sectional ice thickness measurements close to the glacier termini. Our estimates therefore improve on their assumption of uniform ice thicknesses equal to the centerline ice thickness.

[15] The error in the ice thickness at any single measurement point is low (±10 m) and where there is cross over between the RES and IPR flight lines, the ice thickness measurements agree to within this error margin. These data constrain the cross-sectional profiles of the main tidewater calving termini (i.e., Wykeham, Trinity and Cadogan Glaciers) very effectively (e.g., Figure 4). We estimate the error in the cross-sectional areas to be <5%. At Ekblaw glacier, there was very close agreement between RES and IPR measurements made along longitudinal flight lines (<3 m difference at crossover points) but there was a discrepancy in thickness between these and the IPR cross-sectional profile (IPR thicknesses were 171 m thinner) which indicates an error in the cross-sectional profile measurements or postprocessing. These were corrected to match the longitudinal profiles, where these crossed. We therefore assume the error in the Ekblaw cross-sectional areas to be ~10%.

3.2.2. Average Cross-Sectional Velocity, $\bar{v}_{x-sect}$: Measurement and Errors

[16] The mean velocity over a cross section is within a few percent of the mean surface velocity across the glacier width [*Paterson*, 1994, p. 270]. Speckle tracking of synthetic aperture radar (SAR) data measures the displacement of the Earth's surface between successive satellite orbital cycles by comparison of coherent radar images acquired during each cycle [*Gray et al.*, 2001]. It enables the measurement of ice surface velocity in fast-moving areas and can be successful even where visible features are absent. It has been applied in Antarctica [*Gray et al.*, 2001; *Joughin*, 2002], Greenland [*Luckman et al.*, 2003] and the Canadian High Arctic [*Short and Gray*, 2005]. To determine the mean surface velocity across the widths of glacier termini, surface velocities along the RES and IPR transects were extracted from RADARSAT-1-derived speckle tracking velocity data files, presented and discussed in detail by *Short and Gray* [2005]. They discuss the various sources and magnitudes of error in these data and conclude that "...it is difficult to give an overall error estimate for the speckle tracking results, since the errors vary spatially within a dataset depending on the level of coherence, the presence of azimuth streaks, the accuracy of the DEM, local nonsteady state thickness changes, proximity to the stationary reference areas, and whether or not the ice is floating" [*Short and Gray*, 2005, p. 229]. They quote a range of average errors from 14 to 24 m a^{-1} depending on

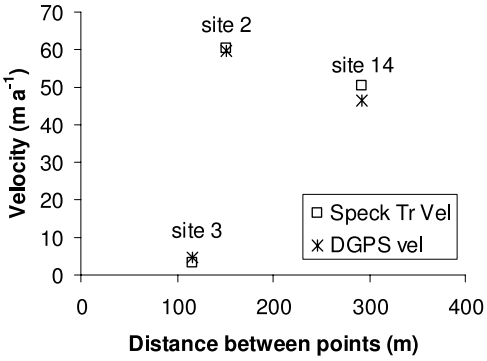

Figure 5. Comparison of annual ground differential GPS velocity measurements made between May 2001 and May 2003 and RADARSAT-1-derived speckle tracking velocities calculated over 24 day periods from February to March 2004 and 2003. DGPS stakes at core sites 2, 3, and 14 (Figure 2).

the acquisition beam mode and image resolution (fine or standard) of the RADARSAT-1 data. Errors for the east flowing glaciers on POW are higher (<30 m a^{-1}) because of an inability to correct for potential tidal effects where the exact position of grounding lines is unknown.

[17] Speckle tracking is applied across pairs of 250 m × 250 m image chips. However, displacement values with poor cross correlation coefficients are rejected, so the actual spatial resolution of reliable velocity values is much less than this. This is particularly true for the terminal areas of fast flowing tidewater glaciers where the RES and IPR cross-sectional profiles were measured. The discontinuous spatial sampling of surface velocity measurements (Figure 4) means that interpolation between measurements is carried out to determine the mean surface velocity across the width of the glacier. To assess the mean velocity error due to the interpolation method, we undertook jackknifing interpolations of surface velocity, whereby individual velocity measurements were systematically omitted from the interpolation. On average, mean surface velocity differences were ∼2% and standard deviations were ∼6% of initial calculated average surface velocity. It is not possible to determine precisely gross interpolation errors across unmeasured portions of the velocity profiles; however we estimate that the total error in the mean velocity over a cross section is <10%. The exception is Ekblaw Glacier where the poor spatial resolution of surface velocity measurements across the width of the glacier terminus meant that the average cross-sectional velocity had to be estimated from the centerline velocity. The theoretical work of *Nye* [1965, Table IIIb] shows that for a nonsliding glacier in a parabolic channel with dimensions similar to Ekblaw Glacier, the average cross-sectional velocity, $\bar{v}_{x-sect}$, is ∼0.6× the centerline surface velocity, v_c. However, *Short and Gray* [2005] show increasing velocity toward the terminus and significant interannual variability along most of the main trunk of the glacier between 2000 and 2003 that indicates that the glacier does slide and so we assume that $\bar{v}_{x-sect}/v_c$ is higher. A ratio of 0.8 is used in our calving flux estimate. This allows for a component of sliding but assumes that deformation is still a significant component since the glacier is grounded all along the cross-section profile. The error for Ekblaw Glacier is therefore estimated to be ∼20%.

[18] A further source of uncertainty is the assumption that the 24-day measurement period, over which the RADARSAT-1 speckle tracking velocities are derived, is representative of the long-term average flow regime. Thirteen differential GPS measurements of annual velocity were made on the ice field over the period April 2001 to May 2003. Three of these velocity stakes overlap closely (<300 m) with data points extracted from speckle tracking velocity files from February to March 2003 and 2004 from the high-elevation regions of the Ekblaw Glacier and Wykeham Glacier catchments respectively. The close agreement between these measurements (Figure 5) suggests that winter velocities are very similar to annual velocities at high elevations, though this may not be true of velocities near tidewater termini where sliding is more likely. None of the glaciers studied in the calving flux estimates below has been identified as a surge type glacier [e.g., *Copland et al.*, 2003]. However, *Short and Gray* [2005] show some acceleration of the main glacier trunks of Ekblaw, Trinity and Wykeham Glaciers during the period 2000–2004 but this was not obvious at the glacier termini where our Q_{flux} estimates were calculated. The lack of termini acceleration could have been due to errors caused by not accounting for tidal influences in the later velocity data and so one could argue that our estimation of Q_{flux} based on 2003 velocities for Ekblaw Glacier and 2004 velocities for Trinity and Wykeham Glaciers might be an overestimate. *Short and Gray* [2005] discuss the possibility that some of these glaciers may exhibit multiyear, periodic pulse-like variations in flow that might fit with *Raymond*'s [1987] suggestion that glaciers in general may display a continuum of pulsating flow regimes, of which surging is an end-member. The flow regimes at higher elevations along these glaciers may have been invariant over the period 2000–2004 but we simply do not have enough long-term flow data from this ice field to determine how large the error is in assuming invariant flow over the entire elevation range of the ice field and over time periods of several decades.

3.2.3. Tidewater Glacier Terminus Changes: Measurement and Errors of Q_{v-loss}

[19] Observations of changes in tidewater glacier terminus positions over approximately the last four decades were based on a comparison of 1:60,000 aerial photography acquired in late July and early August of 1959/1960 by the Government of Canada with Landsat 7 ETM+ panchromatic (15-m resolution) scenes acquired on 13 July 1999 and 2 August 2000 (path 40 rows 4 and 5). Ice margins were digitized for each data set and overlay analysis and raster cartographic techniques were used to detect and quantify area differences between the two data sets. The methodology for this work is essentially the same as that described by *Burgess and Sharp* [2004] for the Devon Island Ice Cap where the minimum error of the area change measurements for an individual drainage basin was estimated to be ±11% for basins with unobscured margins. The same error estimate applies to the estimates presented in this paper.

[20] The Leffert Glacier in the northeast of the ice field and much of the southeast margin are included in the calculation of Q_{v-loss}. The lack of extensive surface crevassing suggests

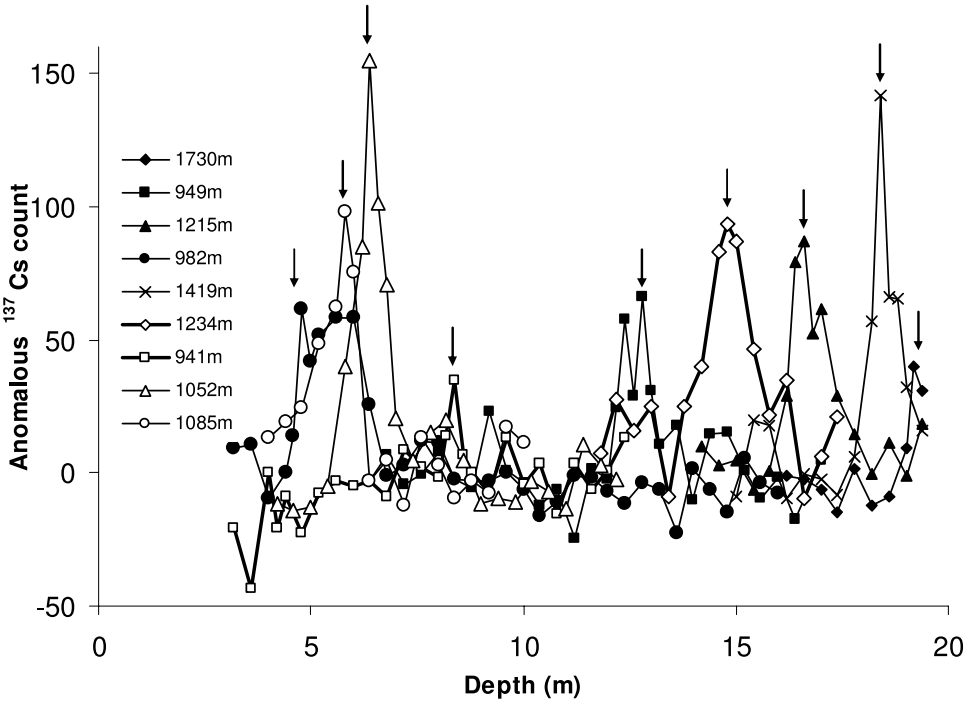

Figure 6. Anomalous ^{137}Cs count rates at depth within northern shallow core boreholes, i.e., after removal of background counts as determined by the polynomial trend line shown in Figure 3a. Bomb peak positions indicated by arrows. Elevations of cores in legend (note that core at 1730 m reached to 1965 depth, i.e., rising limb of 1963 bomb peak).

these glaciers are not as dynamic as the Ekblaw, Cadogan and Trinity/Wykeham glaciers, but they do reach the sea and show significant marginal change since the 1960s. Converting a glacier area change into an ice volume change involves estimating the thickness of ice gained or lost. Ice thickness data are available from RES and IPR transverse transects flown within a few kilometers of the termini of all these catchments. We estimate the total error in ice volume changes caused by changing terminus positions is $\sim \pm 15\%$. We assume a glacier ice density of 900 kg m^{-3} when converting ice volume changes into water volume equivalents.

3.3. Digital Elevation Model

[21] The digital elevation model (DEM) used in this study was a subset of the Canadian Digital Elevation Data set (CDED) produced from the National Topographic System (NTS) 1:250,000 map sheets. These were derived from aerial photography obtained in late July and early August of 1959 and 1960 by the Government of Canada. Vertical accuracy of the DEMs ranges from ±20 m at the glacier margins to ±50 m across interior regions of the ice field [*Burgess and Sharp*, 2004].

4. Surface Mass Balance Results

4.1. Measurements of Net Accumulation From Shallow Ice Cores

[22] The 1963 "bomb" layer was very clearly identified at 12 of the 13 core sites (e.g., Figure 6). At the lowest-elevation ice core site (site 8, 941 m asl), the peak at depth was markedly lower than at other sites. The magnitude of the peaks is a function of both the concentration of ^{137}Cs within the range of the spectrometer detector (~50 cm) and the intensity of the radiation emitted from the strata with the highest concentration of ^{137}Cs. The magnitudes of the peaks do not relate to core densities at peak depths. We cannot determine whether the variation in peak magnitudes relates to: spatial variations in the intensity of fallout; spatial variations in the post depositional snowpack processes of melt, percolation and/or refreezing; small-scale variations in the density structure of the firn around the bomb peak; or variations in the proximity of the detector to the bomb layer strata, given that the measurement resolution was 20 cm.

[23] Shallow ice core-derived b_n estimates for the period 1963–2000/2001 are shown in Table 2. Core site 1, on the central plateau, is at the nominal ice divide, although nunataks and snow covered hills protrude to elevations of just over 2000 m in several locations. As part of a different but related project, the core at this site was returned to the University of Alberta for detailed density, chemical and ^{18}O isotopic analysis to determine the annual layer stratigraphy and accumulation history since 1965. This work gave an average value of 320 kg m^{-2} a^{-1} for b_n, which agrees very closely with our field measurement of 311 kg m^{-2} a^{-1}. The field measurement uncertainty is likely to be higher for lower-elevation sites where the bomb layer is shallower and the firn densities are generally higher. Here, the bomb layer depth resolution of 20 cm will create a higher percentage error in determining mass accumulation. However, the close agreement between laboratory and field measurements of the summit plateau core gives us confidence in our shallow core field measurements of b_n elsewhere and we estimate

Table 2. Average Net SMB, $b_{n\ 63-00/01}$, Derived From Measurements on Shallow Ice Cores[a]

Core Number[b]	Core Elevation (m asl)	$b_{n\ 63-00/01}$ (kg m^{-2} a^{-1})
8 (NW)	941	197
2 (NE)	949	293
14 (SE)	960	332
4 (NE)	982	111
9 (NW)	1052	150
13 (SW)	1056	264
10 (NW)	1085	135
12 (SW)	1100	203
3 (NE)	1215	285
7 (NW)	1234	266
11 (SW, SE)	1350	440
5 (NE)	1419	273
1 (NW, NE)	1730	311

[a]Values relate to the periods 1963–2000 (cores 1–10) or 1963–2001 (cores 11–14). Measurement error is <10%.
[b]Sectors are given in parentheses.

that the long-term net mass balance at a point can be determined with an accuracy of <10%.

4.2. Stake Measurements

[24] Stake measurements of net SMB, b_n, for the year 2002–2003 are shown in Table 3. Snow depths at stakes KR0550 and SP1030 were anomalously high and low respectively. Strong westerly winds were observed to cause localized drifting and scouring in highly sheltered or exposed locations respectively. These stake values are therefore excluded from the subsequent analyses of these data (below) which relates patterns in SMB to larger-scale environmental controls.

4.3. Spatial Patterns of SMB

[25] The relationship between core and stake b_n values and elevation shows strong regional variation (Figure 7). There is a broad pattern of increasing accumulation, lower equilibrium line altitude (ELA) and shallower ablation gradients moving from the northwest to the southeast of the ice field (although there is a paucity of data from the ablation area of the southeast of the ice field where satellite imagery indicates widespread crevassing which restricted travel by snowmobile to a known, safely navigable route, thereby preventing more extensive field measurements). The ELAs in the northeast and southwest sectors of the ice field lie above firn line observations made by Koerner in May and June 1974 [*Koerner*, 1979, Table 4]. The lowest ELA of ~500 m asl in the southeast sector also lies just above what Koerner called a "firn outlier" at 200–400 m asl (Figure 7d).

5. Analyses of Surface Mass Balance

[26] One of the aims of this study is to estimate the contribution of the SMB of the whole of POW, B_n, to the overall mass balance of the ice field. To determine B_n, it is necessary to relate SMB measurements at a point, b_n, to external environmental controls for which the spatial variation across the ice field is known. It is then possible to extrapolate and interpolate b_n across the entire ice field to estimate B_n. There are some obvious problems in attempting this.

[27] First, the spatial coverage of field measurements is limited to areas that could be safely accessed within the two spring field seasons. This leaves the magnitude of b_n in some of the largest drainage basins on the ice field (e.g., Trinity and Wykeham Glaciers) and all of the high coastal mountain ranges to the east largely unconstrained by field data. Second, we have different temporal averages of b_n at different sites, i.e., 37/38 year average net accumulation measurements from ice cores and 1 year average mass balance measurements from stakes. It is therefore desirable to determine how representative are the stake data of the long-term mean and apply a correction factor to them before relating them to environmental controls.

[28] We have both stake and core measurements for four sites (HM1050/core12, KR960/core14, SP1030/core13, and SSUMMIT/core11) and two other pairs of sites where cores and stakes are within <100 m elevation and <10 km distance from each other (WL1100/core9 and WL1300/core7). Net accumulation during 2002/2003 was on average 1.5 (root-mean-square error = 0.2) times greater than the average over the long-term core record. There was no systematic variation in this ratio with elevation. We therefore assume that 2002–2003 net accumulation measurements can be adjusted to fit the long-term data by multiplying by 0.67. Determining a correction for 2002–2003 net mass balance measurements at lower elevations is less straightforward.

[29] *Koerner*'s [2005] review of the long-term mass balance records of several of the Queen Elizabeth Islands (QEI) ice caps found that: interannual variation in winter snow depths is low across the QEI ice caps (our measurements show <6% difference in average winter snow depths below 800 m between May 2002 and May 2003); the variability of mass balance is almost entirely driven by the variability of the summer balance, i.e., a short 2–3 month period; and that warmer summers in the late twen-

Table 3. Stake Measurements of SMB, $b_{n\ 02-03}$, for the Year 2002–2003[a]

Stake Number[b]	Stake Elevation (m asl)	$b_{n\ 02-03}$ (kg m^{-2} a^{-1})
KR0350 (SE)	350	−256
LL400 (NE)	395	−957
HM0450 (SW)	450	−970
KR0550 (SE)	550	448
LL600 (NE)	602	−401
WL610 (NW)	610	−949
HM0750 (SW)	740	−181
WL750 (NW)	747	−499
KR0750 (SE)	750	364
LL800 (NE)	799	−153
SL850 (NW)	850	−22
KR0960 (SE)	960	623
SP1030 (SW)	1030	−0.2
HM1050 (SW)	1056	285
SL1060 (NW)	1060	296
WL1100 (NW)	1094	199
LL1100 (NE)	1105	270
KR1160 (SW)	1160	166
HM1240 (SW)	1240	156
LL1300 (NE)	1308	382
WL1300 (NW)	1310	353
SSUMMIT (SW, SE)	1350	649
LL1500 (NE)	1510	376
POWHI (NW, NE)	2009	153

[a]Measurement error is 10–15%.
[b]Sectors are given in parentheses.

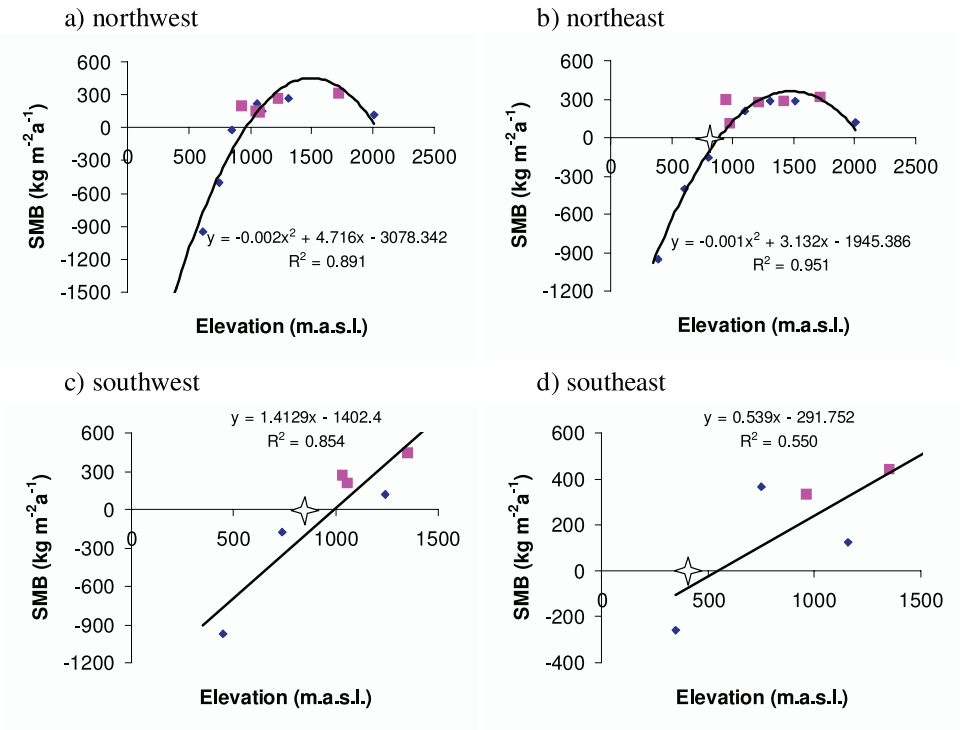

Figure 7. SMB as a function of elevation shown by region: (a) northwest, (b) northeast, (c) southwest, and (d) southeast. Stars indicate elevation of the firn line as identified from shallow core observations undertaken in 1974 [*Koerner*, 1979]. Core and stake measurements are shown by squares and diamonds, respectively.

tieth century caused a downward trend in mass balance. Since our stake mass balance measurements relate to the period May 2002 to May 2003, then temperatures during summer 2002 are critical in determining how ablation during this year compared with the long-term mean values. *Marshall et al.* [2007] recorded near surface air temperature at ablation stakes across the northern sites on POW in summers 2002 and 2001. They found very steep temperature lapse rates in summer 2002 (-5.0°C km^{-1}) compared with 2001 (-3.7°C km^{-1}). Summer 2002 was warmer than 2001 at low elevations but colder than 2001 at altitudes above ~800 m. This is a surprising result since overall, 2002 and 2001 were cool and warm summers, respectively, across the QEI. On Devon Ice Cap, 2001 was the most negative annual mass balance measured in over 40 years of monitoring. Additionally, *Wang et al.*'s [2005] analyses of enhanced resolution QuikSCAT (QSCAT) scatterometer images of the QEI ice masses over the period 2000–2004 showed that melt duration on POW in summer 2002 was anomalously high at low elevations, i.e., below ~800 m, but anomalously low at high elevations relative to the 5 year average over summers 2000–2004 [*Wang et al.*, 2005, Figure 4]. Therefore, the combined effect of higher temperatures and longer melt duration at lower elevations indicates that net ablation in 2002 was higher than the 2000–2004 average. We do not know how 2000–2004 mass balance regime at lower elevations of POW compares with the long-term mean (i.e., 1963–2003), but we can make such a comparison for the northwest sector of Devon Ice Cap, which is the only ice cap to have a mass balance record extending back to 1963. The 2000–2004 mass balance of Devon Ice cap was considerably less negative than the 1963–2003 average (-217 kg m^{-2}a^{-1} and -348 kg m^{-2}a^{-1} respectively; data are from World Glacier Monitoring Service, www.wgms.ch). If the same trends hold for POW, then it is reasonable to assume that net ablation across POW in 2002 may be close to the mean for the period 1963–2003. We therefore apply no correction to stake ablation measurements below 800 m elevation.

5.1. Controls on SMB

[30] SMB across High Arctic ice caps has been clearly related to mean elevation, though the relationship is usually nonlinear [*Dyurgerov*, 2002]. The nonlinearity is probably partly due to the fact that the magnitude of precipitation is often closely related to distance from moisture source [*Koerner*, 1979] as well as to elevation. *Alt* [1979] attributed the existence of the Meighen Ice Cap at unusually low elevations to the existence of melt-suppressing fog caused by cold air masses moving onto the ice cap from the nearby Arctic Ocean. *Koerner* [2005] suggests that fog originating from an increasingly open Jones Sound may also cause melt suppression at the lower elevations of Sverdrup Glacier on the Devon Ice Cap. For POW the main moisture source is the very proximal Smith Sound portion of the NOW polynya (Figure 1). However, *Wang et al.* [2005] showed that mean melt duration across the QEI ice caps depends mainly on surface elevation but also that melt duration decreased with increasing distance from Baffin Bay. This implies that Baffin Bay is a heat source as well as a moisture source.

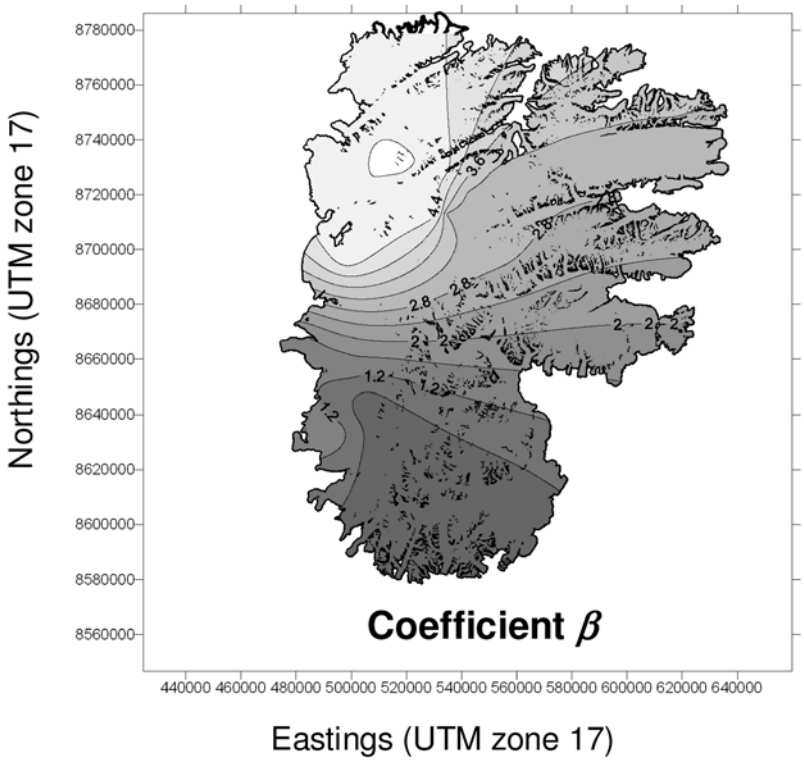

Figure 8. Spatial variation in coefficient β (equation (3)) for case of regional b_n versus z method (explained in text).

[31] Thus, in order to estimate B_n, field measurements of b_n must be related to elevation *and* account for the regional impact on b_n of proximity to moisture/heat sources. There are many different ways this could be carried out. Herein we describe and present the results from two different approaches to determining the spatial pattern of SMB across the whole ice field. Undertaking different analyses helps quantify the uncertainty in B_n that can be attributed to the method of extrapolating B_n from b_n measurements, elevation and regional moisture/heat source influences, as well as from the individual measurement errors and uncertainties associated with b_n and the ice field DEM.

5.2. Regional b_n Versus Elevation Relationship Method

[32] The regional variability in the b_n versus elevation relationship prohibits the extrapolation of a single polynomial regression trend line across the entire ice field. Instead the spatial pattern of b_n was determined from the following analyses.

[33] 1. Regional b_n versus elevation relationships are derived for each of the plots shown in Figures 7a–7d, i.e., northwest, northeast, southwest and southeast sectors of the ice field (see Tables 2 and 3 for sector allocations between core and stake measurements). Relationships have the form

$$b_n = \alpha z^2 + \beta z + \chi, \tag{3}$$

where z is elevation.

[34] 2. Three map grid files were created showing how each of the coefficients, α, β and χ varies across the ice field. This was done by (1) mapping the values of the respective regional coefficients α, β and χ to each regional stake or core location, and (2) interpolating the variation in coefficient values between regions and across the entire ice field using a kriging routine in the Golden Software Surfer program (e.g., Figure 8). Coefficient values are therefore the same at all measurement locations from which that coefficient was derived, but they vary through space beyond regional groupings. Note that the value of coefficient α converges to zero toward southern measurements locations where linear relationships exist between b_n and z (Figures 7c and 7d).

[35] 3. Each coefficient map grid file is multiplied by the DEM grid file, raised to its corresponding power of elevation. This creates three grids, i.e., αz^2, βz and χ, which are then summed to obtain an interpolated, empirically derived map of SMB for the entire ice field.

[36] The accuracy of the resulting SMB grid is assessed by extracting predicted values for b_n at stake or core locations and comparing these with measured values (Table 4).

5.3. Distance to North Open Water (d_{NOW}) Multiple Regression Method

[37] Since distance to moisture/heat source has been identified as a likely control on SMB, multiple regression was carried out of b_n against elevation, z, and distance from the Smith Sound portion of the NOW polynya, d_{NOW} (in kilometers from position shown on Figure 2). Grid files of spatial variations in z (i.e., the POW DEM) and d_{NOW} are substituted into the multiple regression equation using the "Grid-Math" function in Surfer to determine spatial patterns of SMB across POW.

$$b_n = -0.00109\, z^2 + 3.156\, z - 6.317\, d_{NOW} - 880 \tag{4}$$

Table 4. Methods of Extrapolating Field Measurements of SMB Across the Entire Ice Field[a]

Description of Approach	R Measured Versus Predicted	Mean Absolute Error (kg m^{-2} a^{-1})	RMS Error (kg m^{-2} a^{-1})	B_n (km^3 w.e. a^{-1})	Mean-Specific B_n (m w.e. a^{-1})
Combined regional b_n versus z relationships (polynomial and linear)	0.94	107	133	+0.15	+0.008
Multiple regression relating b_n to z^2, z, and d_{NOW}	0.91	132	158	−0.35	−0.018

[a]R value, mean absolute error, and RMS error for predicted b_n versus measured b_n are shown for each extrapolation method. B_n, the total SMB for the entire ice field calculated for each extrapolation method (explained in text) is also shown.

A second-order polynomial relationship with z and a linear relationship with d_{NOW} (equation (4)) gives a good match between predicted and measured values of b_n (Table 4).

5.4. Total SMB of Prince of Wales Icefield

[38] The total SMB for the entire ice field, B_n, was estimated for each extrapolation method by calculating the net "volume" of the SMB grids from which b_n contour maps were created. This was done, following the method of *Mair et al.* [2005], using the Surfer Grid/Volume function that calculates the net volume between a grid surface and a horizontal plane, which, in this case, is where mass balance equals zero. The total net accumulation (positive volume) and net surface ablation (negative volume) are calculated and their sum gives an estimate of B_n (values shown in Table 4).

[39] The value of B_n varies depending on the extrapolation method used but both estimates suggest that SMB is close to zero. The average of the two estimates gives B_n equal to -0.1 km^3 w.e. a^{-1}. The spatial pattern of this average SMB is shown in Figure 9. Total net accumulation is +3 km^3 w.e. a^{-1} and total net ablation is -3.1 km^3 w.e. a^{-1}.

5.5. Errors in B_n Estimate

[40] There are four main errors or uncertainties associated with our estimate of B_n: (1) error or uncertainty associated with different values of B_n resulting from different extrapolation methods; (2) impact of DEM errors and elevation/area changes over past 40 years; (3) measurement error of core and stake b_n values, and (4) uncertainty inherent in the limited temporal and spatial sampling of b_n.

[41] We can quantify the first three errors. First, the error associated with different extrapolation methods is taken as half of the difference between the two B_n estimates, which equals ±0.25 km^3 w.e. a^{-1}. Second, the effect of the DEM error is determined by uniformly changing elevations by plus and minus 30 m and increases the error by ~30%. This uncertainty also accounts for changes in basin hypsometry that may have occurred over the past ~40 years. Assuming

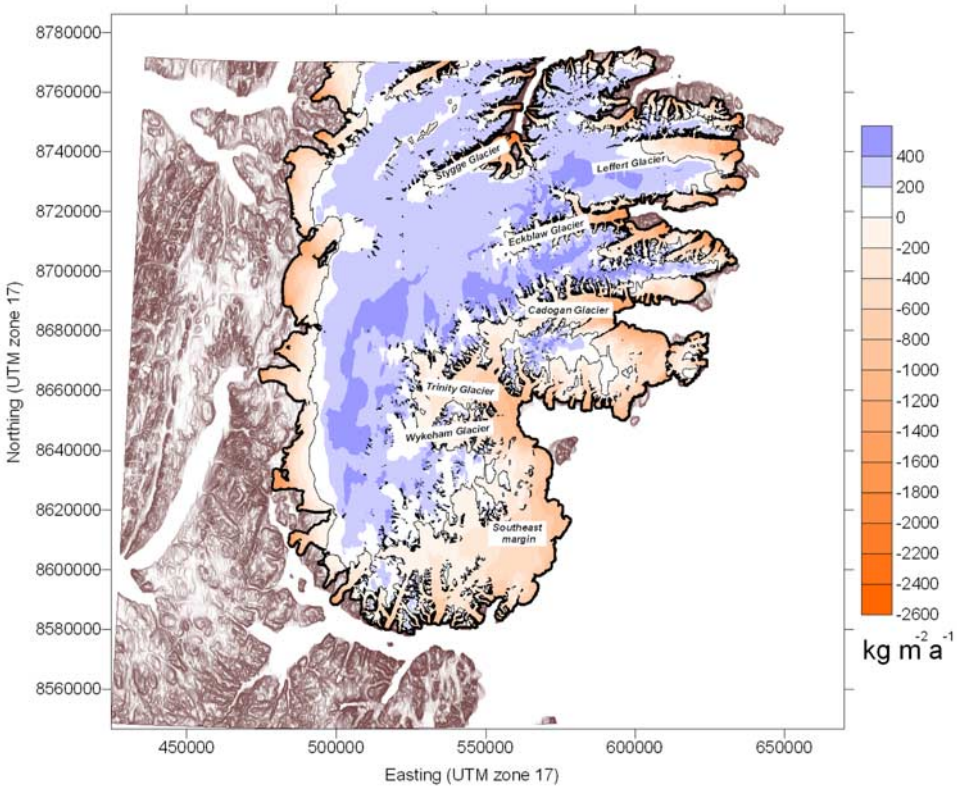

Figure 9. Spatial pattern of SMB across Prince of Wales Icefield as determined by averaging the two extrapolation approaches (explained in text). ELA is highlighted.

Table 5. Iceberg Calving Totals and Components Q_{flux} and Q_{v-loss} by Glacier Basin[a]

Glacier Basin	Q_{flux} (km^3 w.e. a^{-1})	Q_{v-loss} (km^3 w.e. a^{-1})	Q_{Total} Calving Total (km^3 w.e. a^{-1})
Leffert	-	−0.01 ± 0.002	−0.01 ± 0.002
Cadogan	−0.08 ± 0.012	−0.02 ± 0.003	−0.10 ± 0.012
Ekblaw	−0.22 ± 0.044	+0.014 ± 0.002 (terminal advance)	−0.21 ± 0.044
Trinity and Wykeham	−1.35 ± 0.2	−0.21 ± 0.03	−1.56 ± 0.2
SE Margin	-	−0.04 ± 0.006	−0.04 ± 0.006
Totals	−1.65 ± 0.21	−0.27 ± 0.03	−1.92 ± 0.21

[a]Q_{Total} is the iceberg calving totals, Q_{flux} is the annual volume of ice flux discharged at the tidewater termini, and Q_{v-loss} is the volume loss due to the observed change of terminus position.

constant rates of change, ice surface elevations measured along four transects across the ice field from NASA laser altimetry surveys in 1995 and 2005 suggest that changes appear to have been limited to less than ±20m in magnitude since 1960. Similarly, areal changes over this period of time are not likely to have significantly influenced the long-term net mass balance values, as the ice field has decreased in area by less than 1% over the past 40 years [*Sharp et al.*, 2004]. Third, the measurement error in b_n values increases the error further by ∼15%. The fourth uncertainty can only be determined through improved coverage of field measurements. Thus, including the quantifiable errors, B_n is −0.1 ± 0.4 km^3 w.e. a^{-1}.

6. Iceberg Calving

[42] The rate of ice calved directly into the ocean due to flux at the tidewater margins is estimated to be 1.65 ± 0.21 km^3 w.e. a^{-1} (Table 5). Volume loss due to retreat of the tidewater termini is 0.27 ± 0.03 km^3 w.e. a^{-1} bringing the total mass loss due to calving to 1.92 ± 0.21 km^3 w.e. a^{-1}.

7. Overall Mass Balance of POW Icefield

[43] By subtracting the iceberg calving total, Q_{Total}, from the average SMB, B_n (i.e., −0.1 ± 0.4 km^3 w.e. a^{-1} minus 1.9 ± 0.2 km^3 w.e. a^{-1}), the overall mass balance of POW can be estimated as −2 ± 0.45 km^3 w.e. a^{-1} equivalent to a mean-specific mass balance of −0.1 m w.e. a^{-1}. The real error margin may be larger than this since unquantifiable uncertainties have been identified earlier that could increase the error.

8. Discussion

8.1. Surface Mass Balance

[44] Both approaches to extrapolating b_n across the entire ice field indicate that the SMB of the Prince of Wales Icefield is very close to zero. This is unusual for the region where SMB across a number of ice masses has shown a trend toward increasingly negative values [*Koerner*, 2005]. This is most likely due to proximity to the NOW polynya, a year-round nearby source of moisture. The marked regional variation in SMB-elevation relationships shown in Figure 7 and the outcome of multiple regression analyses shown in equation (4), indicates that melt is suppressed and/or accumulation is increased with proximity to the NOW polynya. It is possible that low-lying fog originating from the NOW polynya may cause a melt suppression effect during summer across the southeastern region of POW similar to that discussed earlier for Meighen Ice Cap [*Alt*, 1979] and low elevations of northwest Devon Ice Cap [*Koerner*, 2005].

[45] However, snow depths measured in May 2002 and 2003 show much greater accumulation across the eastern catchments facing the NOW polynya. This may suggest that enhanced accumulation, rather than suppressed ablation, is the more likely marine control on SMB. *Krabill et al.* [2000] measured anomalously high thickening rates across a low-lying isolated icecap in the extreme northeast of Greenland, located close to the North East Water polynya, and attributed the thickening as a response to locally increased snowfall. The survey period of their airborne laser altimetry measurements (1994–1999) included 2 years with exceptionally large polynyas. Similarly, *Braithwaite* [2005] speculated that reduced sea ice cover surrounding the arctic islands could cause very large changes in mass balance of arctic ice caps through higher annual precipitation and lower annual temperature variability, i.e., more maritime conditions. *Marshall et al.* [2007] noted seasonal and spatial variations in lapse rates across east and west facing catchments of the southern POW. Temperatures at lower elevations across the eastern catchments were higher (i.e., lapse rates were more negative) than in the west during winter/spring (i.e., December–May) on account of the potential impact of the NOW providing a source of sensible heat. However, in the summer (June–November) temperatures at lower elevations across the eastern catchments were lower (i.e., lapse rates were less negative) than in the west. It is therefore feasible that both increased winter/spring accumulation and suppressed summer ablation may be responsible for the regional variations in SMB observed. Whatever the precise mechanism, the shallow mass balance gradients of the southeastern regions of POW appear to show the effects of a strong marine control.

8.2. Iceberg Calving

[46] Over 97% of all tidewater calving is attributed to the Trinity/Wykeham, Ekblaw and Cadogan glaciers. Satellite imagery and areal photogrammetry confirm that these are the only glaciers that appear to produce significant quantities of icebergs. It is worth noting that the Stygge Glacier that drains a large catchment in the north of POW and flows north into Jökull Fiord shows little visible sign of iceberg calving, has not changed its terminal position over the last four decades and has a relatively thin (<100m), very slow moving terminus (<25 m a^{-1}, i.e., within the error margin).

[47] Over 80% of the mass loss due to iceberg calving is attributed to calving at the combined tidewater terminus of the Trinity and Wykeham Glaciers (Table 5). These large

glaciers drain most of the ice from the southeast sector of the ice field through a complex topography of mountain ranges and nunataks. RES measurements from 2000 show that almost the entire ablation area of Trinity Glacier, i.e., up to ~50 km from the terminus, is grounded below sea level. This dominance of one major source of mass loss from a calving terminus is a feature of other Canadian High Arctic ice masses, notably the Belcher Glacier on the Devon island Ice Cap [*Burgess et al.*, 2005] and the Eugenie Glacier on the Agassiz Ice Cap [*Williamson et al.*, 2008]. Ekblaw Glacier advanced over the period 1960–2000 but still lost considerable mass through calving on account of its high velocities (centerline surface velocity of ~330 m a^{-1}) and very thick ice (>500 m) causing high ice flux at the terminus. Our estimates of calving mass loss for Trinity, Wykeham and Ekblaw Glaciers are lower than those calculated by *Short and Gray* [2005] despite the fact that we have used their estimates of surface velocity. This is most likely because *Short and Gray* [2005] assumed a uniform ice thickness across the glacier termini equal to the centerline ice thicknesses which would overestimate the cross-sectional area compared with this study. In addition their estimate of the mass loss due to the changes in the tidewater terminus positions of Trinity and Wykeham Glaciers is much higher (-1.1 km^3 w.e. a^{-1}) than our estimate (-0.21 km^3 w.e. a^{-1}). Their estimates were based upon comparison of 1960 aerial photography with satellite imagery from 2003 and 2004 (rather than with our comparison of 1959/60 photography with 1999/2000 satellite imagery) and showed that Trinity Glacier was retreating rapidly while Wykeham was advancing. These different results may simply reflect periodic variability in calving rates rather than being indicative of longer-term trends. The POW decreased in surface area by only 0.7% over the period 1959–2000 [*Sharp et al.*, 2004]. This compares with a 2.4% reduction of the Devon Ice Cap [*Burgess and Sharp*, 2004], and an average area loss of 2.1% for all major ice masses across the entire QEI over the same time interval. Thus, over approximately the last four decades some glaciers have advanced, some have retreated and across most of the ice field there was very little change in marginal position. These observations suggest there has not been a widespread increase in retreat across the ice field in recent years and reduces the possibility that our calving estimates are affected by a systematic bias.

8.3. Overall Mass Balance, B_n

[48] A good way of verifying our B_n estimate would be to compare average changes in surface elevation between 1995 and 2005, measured across four east-west transects during NASA's airborne laser altimetry campaigns (i.e., a continuation of the work presented for 1995–2000 by *Abdalati et al.* [2004]), with catchment scale-specific mass balances derived from this study. Initial analysis of one section of one of the NASA laser transects, which follows the entire length of the Ekblaw Glacier, reveals an average ice elevation change of +0.77 m along the glacier centerline. This value does not represent a rigorous estimate of specific mass balance of the basin since that would require extrapolation of the elevation changes over the area of the glacier and division by the total basin area. Spatial extrapolation of centerline elevation change data to estimate mean-specific mass balance involves assumptions about the spatial uniformity of elevation change and surface density across elevation bands. This will form the focus of a further study carried out for several basins across POW and is beyond the scope of this paper. However, the analyses in this paper predict a total SMB of the Ekblaw Glacier (as defined by GLIMS catchment boundaries) of +0.31 km^3 w.e. a^{-1}, a total calving mass loss of -0.21 km^3 w.e. a^{-1} and so giving an overall mass balance of +0.1 km^3 w.e. a^{-1}, equivalent to a mean-specific balance of +0.067 m w.e. a^{-1}. This is equivalent to +0.74 m ice elevation change over a 10 year period. The level of agreement between this value and the average elevation change along the glacier centerline is encouraging given the different methods used and the different spatial scale of measurement involved in each estimate.

[49] The specific mass balance of POW derived in this study (-0.1 m w.e. a^{-1}) is close to the most recent estimate from the Devon Ice Cap of -0.15 m w.e. a^{-1} [*Burgess and Sharp*, 2008]. The relatively low rate of shrinkage of the POW may reflect the important role of ice dynamics on the geometry of this ice field. Efficient ice transport toward the margins of many POW basins likely inhibits terminus retreat due to surface melting alone, thereby resulting in rates of area loss that are not proportional to the net mass balance across these regions.

[50] To estimate the contribution of POW to global eustatic sea level rise we must consider that only a fraction (4%) of the Q_{v-loss} calving component actually causes sea level rise, i.e., that fraction which is due to thicker ice than that required for hydrostatic equilibrium with the ocean. Consequently, we estimate that POW contributed ~0.005 mm a^{-1} of global eustatic sea level rise averaged over the period 1963–2003.

9. Conclusions

[51] In this paper, we have estimated the overall mass balance of the Prince of Wales Icefield (POW), central Ellesmere Island, from the sum of SMB and iceberg calving.

[52] The net SMB across the Prince of Wales Icefield is determined from analyses of shallow ice core measurements of net accumulation and stake measurements of annual mass balance. Extrapolation of point measurements is accomplished using relationships between surface balance, elevation and distance from the moisture/heat source in the NOW polynya. Two different approaches indicate that the SMB of the ice field is close to zero.

[53] The contribution of iceberg calving to the overall mass balance was calculated from estimates of (1) the volume of ice discharged at the major tidewater glacier termini per annum and (2) the volume loss or gain due to the observed change of termini position per annum. Iceberg calving plays a critical role in determining that the overall mass balance of the Prince of Wales Icefield is clearly negative (-2 ± 0.45 km^3 w.e. a^{-1}). The estimated contribution of POW to global eustatic sea level rise averaged over the period 1963–2003 of 0.005 mm a^{-1} is similar to previous estimates from the Devon Island Ice Cap [*Mair et al.*, 2005; *Burgess and Sharp*, 2008]. This study also supports previous research that has identified iceberg calving as an important part of the overall mass balance equation for

Arctic ice caps and glaciers [*Dowdeswell et al.*, 2002, 2008; *Dowdeswell and Hagen*, 2004; *Burgess et al.*, 2005; *Williamson et al.*, 2008].

[54] This paper provides the first estimate of the overall mass balance of one of the largest Arctic ice masses in the northern hemisphere outside of the Greenland Ice Sheet. Errors and uncertainties reflect the paucity of field data from this remote region of the Canadian High Arctic. To significantly improve our estimate would require the continuation of field programs of mass balance and ice dynamics measurements, including the acquisition of more repeat airborne altimetry flight line data. Modeling mass balance across an ice mass such as POW would be a challenge given the sensitivity of accumulation to local moisture sources, the importance of iceberg calving to total ablation, the possibility of surging glaciers [*Copland et al.*, 2003] and the limited extent of meteorological or field data for calibration and validation. Existing satellite radar altimetry cannot resolve surface elevation change effectively for ice masses of the scale and topographic complexity of POW. Thus we may have to wait until the next generation of satellite radar altimeters are launched, e.g., the European Space Agency's CryoSat2, to substantially improve our estimates of mass balance over ice masses like POW.

[55] **Acknowledgments.** D.M. acknowledges the support of the Leverhulme Trust and the Canadian Circumpolar Institute. D.B. received an IPS-2 scholarship from the Natural Sciences and Engineering Research Council (NSERC), Canada, and Land Data Technologies Inc. M.S. and S.M. received discovery and equipment grants from NSERC and funding from the Meteorological Service of Canada (CRYSYS program). J.A.D. acknowledges support from the John Ellerman Foundation. Funding for the acquisition, analysis, and interpretation of airborne radio echo sounding data was provided by Natural Environment Research Council, United Kingdom, grant GR3/12469 and the European Union SPICE project. We thank Naomi Short and Lawrence Gray (Canada Centre for Remote Sensing) for providing speckle tracking data files and Prasad Gogineni (University of Kansas), Bill Krabill (NASA-Wallops), Mike Demuth (GSC-Glaciology), and the Canadian Space Agency Government Research Initiative Program for efforts toward collecting the ice-penetrating radar and airborne laser data. Essential logistical support in the field was provided by the Polar Continental Shelf Project, Natural Resources, Canada (project 602-01). David Lewis and Faron Anslow provided valuable field assistance to S.M. during the 2002 and 2003 field seasons. The late Roy Koerner provided helpful comments on an earlier version of this paper. We thank the Nunavut Research Institute and the Communities of Grise Fjord and Resolute Bay for permission to work on Ellesmere Island. The insightful reviews of A. Arendt; an anonymous reviewer; and the associate editor, M. Truffer, helped to substantially improve this paper.

References

Abdalati, W., W. Krabill, E. Frederick, S. Manizade, C. Martin, J. Sonntag, R. Swift, R. Thomas, J. Yungel, and R. Koerner (2004), Elevation changes of ice caps in the Canadian Arctic Archipelago, *J. Geophys. Res.*, *109*, F04007, doi:10.1029/2003JF000045.

Alt, B. T. (1979), Investigation of summer synoptic climate controls on the mass balance of Meighen ice cap, *Atmos. Ocean*, *17*(3), 181–199.

Braithwaite, R. J. (2005), Mass balance characteristics of Arctic glaciers, *Ann. Glaciol.*, *42*, 225–229, doi:10.3189/172756405781812899.

Burgess, D. O., and M. J. Sharp (2004), Recent changes in areal extent of the Devon ice cap, Nunavut, Canada, *Arct. Antarct. Alp. Res.*, *36*(2), 261–271.

Burgess, D., and M. J. Sharp (2008), Recent changes in thickness of the Devon Island ice cap, Canada, *J. Geophys. Res.*, *113*, B07204, doi:10.1029/2007JB005238.

Burgess, D. O., M. J. Sharp, D. W. F. Mair, J. A. Dowdeswell, and T. J. Benham (2005), Flow dynamics and iceberg calving rates of the Devon ice cap, Nunavut, Canada, *J. Glaciol.*, *51*, 219–230, doi:10.3189/172756505781829430.

Colgan, W., J. Davis, and M. Sharp (2008), Is the high-elevation region of the Devon ice cap thickening?, *J. Glaciol.*, *54*, 428–436, doi:10.3189/002214308785837084.

Copland, L., M. J. Sharp, and J. A. Dowdeswell (2003), The distribution and flow characteristics of surge-type glaciers in the Canadian High Arctic, *Ann. Glaciol.*, *36*, 73–81, doi:10.3189/172756403781816301.

Dowdeswell, J. A., and J. O. Hagen (2004), Arctic ice caps and glaciers, in *The Mass Balance of the Cryosphere: Observations and Modelling of Contemporary and Future Changes*, edited by J. L. Bamber and A. J. Payne, pp. 527–558, Cambridge Univ. Press, Cambridge, U. K.

Dowdeswell, J. A., et al. (1997), The mass balance of circum-Arctic glaciers and recent climate change, *Quat. Res.*, *48*, 1–14, doi:10.1006/qres.1997.1900.

Dowdeswell, J. A., et al. (2002), Form and flow of the Academy of Sciences Ice Cap, Severnaya Zemlya, Russian High Arctic, *J. Geophys. Res.*, *107*(B4), 2076, doi:10.1029/2000JB000129.

Dowdeswell, J. A., T. J. Benham, M. R. Gorman, D. Burgess, and M. J. Sharp (2004), Form and flow of the Devon Island ice cap, Canadian Arctic, *J. Geophys. Res.*, *109*, F02002, doi:10.1029/2003JF000095.

Dowdeswell, J. A., T. J. Benham, T. Strozzi, and J. O. Hagen (2008), Iceberg calving flux and mass balance of the Austfonna ice cap on Nordaustlandet, Svalbard, *J. Geophys. Res.*, *113*, F03022, doi:10.1029/2007JF000905.

Dunphy, P. P., and J. E. Dibb (1994), ^{137}Cs gamma-ray detection at Summit, Greenland, *J. Glaciol.*, *40*, 87–92.

Dyurgerov, M. B. (2002), Glacier mass balance and regime: Data of measurements and analysis, *Occas. Pap. 55*, Inst. of Arctic and Alpine Res., Univ. of Colo., Boulder, Colo.

Dyurgerov, M. B., and M. F. Meier (2005), Glaciers and the changing Earth system: A 2004 snapshot, *Occas. Pap. 58*, Inst. of Arctic and Alpine Res., Univ. of Colo., Boulder, Colo.

Gray, A. L., N. Short, K. E. Mattar, and K. C. Jezek (2001), Velocities and flux of the Filchner Ice Shelf and its tributaries determined from speckle tracking interferometry, *Can. J. Rem. Sens.*, *27*(3), 193–206.

Intergovernmental Panel on Climate Change (2007), *Climate Change 2007: The Physical Science Basis: Working Group I Contribution to the Fourth Assessment Report of the IPCC*, edited by S. Solomon et al., Cambridge Univ. Press, New York.

Joughin, I. (2002), Ice-sheet velocity mapping: A combined interferometric and speckle tracking approach, *Ann. Glaciol.*, *34*, 195–201, doi:10.3189/172756402781817978.

Joughin, I., I. M. Howat, M. Fahnestock, B. Smith, W. Krabill, R. B. Alley, H. Stern, and M. Truffer (2008), Continued evolution of Jakobshavn Isbrae following its rapid speedup, *J. Geophys. Res.*, *113*, F04006, doi:10.1029/2008JF001023.

Koerner, R. M. (1977), Ice thickness measurements and their implications with respect to past and present ice volumes in the Canadian High Arctic ice caps, *Can. J. Earth Sci.*, *14*, 2697–2705.

Koerner, R. M. (1979), Accumulation, ablation and oxygen isotope variations on the Queen Elizabeth Islands ice caps, Canada, *J. Glaciol.*, *22*, 25–41.

Koerner, R. M. (2005), Mass balance of glaciers in the Queen Elizabeth Islands, Nunavut, Canada, *Ann. Glaciol.*, *42*, 417–423, doi:10.3189/172756405781813122.

Krabill, W., W. Abdalati, E. Frederick, S. Manizade, C. Martin, J. Sonntag, R. Swift, R. Thomas, W. Wright, and J. Yungel (2000), Greenland Ice Sheet: High-elevation balance and peripheral thinning, *Science*, *289*, 428–430, doi:10.1126/science.289.5478.428.

Luckman, A., T. Murray, H. Jiskoot, H. Pritchard, and T. Strozzi (2003), ERS SAR feature-tracking measurement of outlet glacier velocities on a regional scale in east Greenland, *Ann. Glaciol.*, *36*, 129–134, doi:10.3189/172756403781816428.

Mair, D., D. Burgess, and M. Sharp (2005), Thirty-seven year mass balance of Devon ice cap, Nunavut, Canada, determined by shallow ice coring and melt modeling, *J. Geophys. Res.*, *110*, F01011, doi:10.1029/2003JF000099.

Marshall, S. J., M. J. Sharp, D. O. Burgess, and F. S. Anslow (2007), Near-surface-temperature lapse rates on the Prince of Wales Icefield, Ellesmere Island, Canada: Implications for regional downscaling of temperature, *Int. J. Climatol.*, *27*, 385–398, doi:10.1002/joc.1396.

Mundy, C. J., and D. G. Barber (2001), On the relationship between the spatial patterns of sea-ice type and the mechanisms which create and maintain the North Water (NOW) polynya, *Atmos. Ocean*, *39*(3), 327–341.

Nye, J. F. (1965), The flow of a glacier in a channel of rectangular, elliptic or parabolic cross-section, *J. Glaciol.*, *5*, 661–690.

O'Neel, S., W. T. Pfeffer, R. Krimmel, and M. Meier (2005), Evolving force balance at Columbia Glacier, Alaska, during its rapid retreat, *J. Geophys. Res.*, *110*, F03012, doi:10.1029/2005JF000292.

Paterson, W. S. B. (1994), *The Physics of Glaciers*, 3rd ed., 480 pp., Pergamon, Oxford, U. K.

Paterson, W. S. B., and N. Reeh (2001), Thinning of the ice sheet in northwest Greenland over the past forty years, *Nature*, *414*, 60–62, doi:10.1038/35102044.

Raymond, C. F. (1987), How do glaciers surge?: A review, *J. Geophys. Res.*, *92*(B9), 9121–9134, doi:10.1029/JB092iB09p09121.

Rignot, E., and S. S. Jacobs (2002), Rapid bottom melting widespread near Antarctic Ice Sheet grounding lines, *Science*, *296*, 2020–2023, doi:10.1126/science.1070942.

Rignot, E., and K. Steffen (2008), Channelized bottom melting and stability of floating ice shelves, *Geophys. Res. Lett.*, *35*, L02503, doi:10.1029/2007GL031765.

Sharp, M., L. Copland, K. Filbert, D. Burgess, and S. Williamson (2004), Recent changes in the extent and volume of Canadian Arctic glaciers, *Rep. GD-32*, Natl. Snow and Ice Data Cent., Boulder, Colo.

Short, N. H., and A. L. Gray (2005), Glacier dynamics in the Canadian High Arctic from RADARSAT-1 speckle tracking, *Can. J. Rem. Sens.*, *31*(3), 225–239.

Steffen, K. (1985), Warm water cells in the North Water, northern Baffin Bay during winter, *J. Geophys. Res.*, *90*(C5), 9129–9136, doi:10.1029/JC090iC05p09129.

Wang, L., M. J. Sharp, B. Rivard, S. Marshall, and D. Burgess (2005), Melt season duration on Canadian Arctic ice caps, 2000–2004, *Geophys. Res. Lett.*, *32*, L19502, doi:10.1029/2005GL023962.

Williamson, S. N., M. J. Sharp, J. A. Dowdeswell, and T. J. Benham (2008), Iceberg calving rates from northern Ellesmere Island ice caps, Canadian Arctic, 1999–2003, *J. Glaciol.*, *54*, 391–400, doi:10.3189/002214308785837048.

T. Benham and J. A. Dowdeswell, Scott Polar Research Institute, University of Cambridge, Lensfield Road, Cambridge CB2 1ER, UK.

D. Burgess, Canada Centre for Remote Sensing, Natural Resources Canada, 588 Booth Street, Ottawa, ON K1A 0Y7, Canada.

F. Cawkwell, Department of Geography, University College Cork, Cork, UK.

D. Mair, Department of Geography and Environment, School of Geosciences, University of Aberdeen, Aberdeen AB24 3UF, UK. (d.mair@abdn.ac.uk)

S. Marshall, Department of Geography, University of Calgary, 2500 University Drive NW, Calgary, AB T2N 1N4, Canada.

M. Sharp, Department of Earth and Atmospheric Sciences, University of Alberta, Edmonton, AB T6G 2E3, Canada.